Modulation of precipitation by conditional symmetric instability release

Atmospheric Research 185 (2016) 186–201

Contents lists available at ScienceDirect

Atmospheric Research

journal homepage: www.elsevier.com/locate/atmosres

Modulation of precipitation by conditional symmetric instability release

Michael R. Glinton[a], Suzanne L. Gray[a,*], Jeffrey M. Chagnon[a,1], Cyril J. Morcrette[b]

[a]Department of Meteorology, University of Reading, Reading, UK
[b]Met Office, Exeter, UK

ARTICLE INFO

Article history:
Received 27 May 2016
Received in revised form 17 October 2016
Accepted 20 October 2016
Available online 25 October 2016

Keywords:
Conditional symmetric instability
Slantwise convective available potential energy
Convective available potential energy
Vertically integrated extent of realisable symmetric (VRS) instability

ABSTRACT

Although many theoretical and observational studies have investigated the mechanism of conditional symmetric instability (CSI) release and associated it with mesoscale atmospheric phenomena such as frontal precipitation bands, cloud heads in rapidly developing extratropical cyclones and sting jets, its climatology and contribution to precipitation have not been extensively documented. The aim of this paper is to quantify the contribution of CSI release, yielding slantwise convection, to climatological precipitation accumulations for the North Atlantic and western Europe. Case studies reveal that CSI release could be common along cold fronts of mature extratropical cyclones and the North Atlantic storm track is found to be a region with large CSI according to two independent CSI metrics. Correlations of CSI with accumulated precipitation are also large in this region and CSI release is inferred to be occurring about 20% of the total time over depths of over 1 km. We conclude that the inability of current global weather forecast and climate prediction models to represent CSI release (due to insufficient resolution yet lack of subgrid parametrization schemes) may lead to errors in precipitation distributions, particularly in the region of the North Atlantic storm track.

1. Introduction

As well as being important on timescale of hours to days ahead, accurate predictions of the location and intensity of precipitation are of great value further into the future. Although individual storms and high precipitation-accumulation events can not be predicted months in advance, seasonal and decadal prediction systems are increasingly being used to provide projections of how the statistical distribution of precipitation will vary in the months and years ahead (e.g. MacLachlan et al., 2015). Improving the ability to capture the statistical properties of precipitation, including the variations in intensity and spatial coverage, requires representation of, and so an understanding of, all the atmospheric processes that modulate precipitation distributions. The increased physical understanding then needs to be incorporated into the models and tools used when producing projections for the future.

Hobbs (1978) discussed how the precipitation near cold fronts sometimes organises into multiple bands. Bennetts and Hoskins (1979) coined the term conditional symmetric instability (CSI) as an extension of symmetric instability, which had been studied for example by Ooyama (1966) and Stone (1966). They then focused meteorological interest on CSI by suggesting it could be one of the mechanisms responsible for the banding of frontal precipitation on horizontal scales of order 50 km in extratropical cyclones. The aim of this study is to quantify the modulation of surface precipitation in the extratropics due to the release of CSI. Results will indicate whether a slantwise convection scheme would benefit numerical models used for seasonal forecasting and decadal and climate prediction. This aim is motivated by the relevance of CSI release to mesoscale weather phenomena in extratropical cyclones.

Schultz and Schumacher (1999) provide a comprehensive overview of CSI including references to many case studies of events. In summary, CSI is a type of moist instability in which the atmosphere is unstable to cross-frontal slantwise motions, even though it is stable to small perturbations in the vertical and in the horizontal (i.e. stable to conditional instability (CI) and inertial instability (II), respectively). These three types of local atmospheric instability are related. For example, Xu and Clark (1985) demonstrate the similarity between II and the dry forms of CI and CSI with respect to their local dynamics. CSI occurs locally where the environmental lapse rate lies between those of the moist- and dry-adiabatic lapse rates along an absolute momentum surface (as summarised in Table 1 of Schultz and Schumacher (1999)).

Slantwise conditional available potential energy (SCAPE), analogous to conditional available potential energy (CAPE) for CI, is a parcel-derived metric for the potential energy available for conversion to kinetic energy from CSI release (see derivation in Chapter 12

* Corresponding author.
[1] Now at Florida State University, Tallahassee, USA.

http://dx.doi.org/10.1016/j.atmosres.2016.10.013
0169-8095/

of Emanuel (1994) and Section 2.3). SCAPE can be used to infer CSI release if it is diagnosed as existing where ascent is likely to be occurring, such as overlapping a surface front where frontal circulations can lift unstable parcels. CSI can also be diagnosed as occurring where the saturated form of moist potential vorticity (MPV) is negative, and the atmosphere is inertially and conditionally stable. The diagnostic for the vertically integrated extent of realisable symmetric (VRS) instability introduced by Dixon et al. (2002) is based on a form of MPV (see Section 2.4 for more details). An obstacle to assessing the climatological role of CSI release arises because these diagnostics are derived for idealised two-dimensional flow and their interpretation for a realistic, multi-scale, evolving flow is not straightforward. For a case study, CSI release can be inferred by examining the evolution of the instability and flow fields. An alternative approach is taken in this study: the role of CSI release is investigated by quantifying climatological relationships between CSI and weather and by linking the statistical properties of seasonal CSI metrics with the climatological features of extratropical cyclones such as the North Atlantic storm track.

Observational evidence for frontal precipitation banding by CSI release is presented by Bennetts and Sharp (1982) who found that such bands occurred on 80% of the occasions when they were predicted using a diagnostic for CSI based on a derived growth rate for the instability. However, other studies have found a weaker relationship between CSI and precipitation bands e.g., Novak et al. (2010) found CSI to be observed one-third to one-half less often than CI near the time of band formation within the comma head of northeast United States cyclones and Thorpe and Emanuel (1985) found that frontogenesis occurs more rapidly (and with narrower updraughts) as the stability to slantwise convection is reduced to small values, leading them to suggest that it may be difficult to distinguish frontal from slantwise convective circulations in observations of bands. CSI release has also been associated with rapid cyclone development (Shutts, 1990b). Browning (2004) coined the term 'sting jet' to describe the strong near-surface winds found at the end of the hook-shaped cloud head seen in the satellite imagery of rapidly developing cyclones and speculated that CSI release may be responsible for strengthening the wind speeds in this region. Korty and Schneider (2007) proposed that CSI release is one of the mechanisms contributing to ocean-atmosphere coupling. Specifically, they argued that sea-surface-temperature anomalies can be transmitted from the ocean surface to the free troposphere via the neutral slantwise moist adiabatic lapse rate that results from the release of CSI.

Considering criteria for the numerical modelling of the slantwise circulations resulting from CSI release in the atmosphere, Persson and Warner (1991) showed that vertical grid spacing is as important as horizontal grid spacing for resolving slantwise circulations and that spurious gravity waves are a consequence of a vertical grid spacing that is too coarse. Lean and Clark (2003) showed that small-scale slantwise circulations diagnosed from dropsonde data can be resolved with the Met Office Unified Model configured with a 2-km horizontal grid spacing and 90 vertical levels. Motivated by the insufficient resolution of operational numerical weather prediction models at the time, Lindstrom and Nordeng (1992) implemented a slantwise convection parametrization scheme in a three-dimensional primitive equation model with 40-km and 80-km horizontal grid spacing and found the slantwise convection scheme narrowed and intensified the frontal precipitation bands at both resolutions such that they became closer to the observed precipitation amounts. Balasubramanian and Yau (1994) also implemented a slantwise convection parametrization scheme, in this case in a two-layer primitive equation model with 100-km grid spacing. Their aim was to determine the importance of slantwise convection in the explosive development of cyclones and they found that it played a more dominant role than stable condensation in the development of the warm front; the bent-back warm front was found to have a critical role in the explosive cyclogenesis. Despite these studies, it remains unclear whether a slantwise convection scheme would benefit (current day) coarser resolution numerical weather and climate prediction models such as those used for seasonal forecasting and decadal and climate prediction. The purpose of this paper is to show that CSI is climatologically associated with extratropical cyclones and to quantify this relationship. This provides evidence that a failure to represent CSI release in global-scale models could result in errors to the climatological structure and magnitude of the output precipitation field. These errors may be manifest as either an underestimation of precipitation amounts in extratropical cyclones (Lindstrom and Nordeng (1992) found that implementation of a slantwise convection scheme in a coarse resolution case study simulation led to a doubling of the precipitation totals) or, for models tuned to produce realistic precipitation totals, a displacement of the precipitation regions within extratropical cyclones.

In Section 2 the ERA-Interim dataset used and calculations of one metric for CI and two metrics for CSI, SCAPE and VRS instability, are described. Accumulated precipitation over the United Kingdom (UK) is correlated with CAPE and SCAPE in Section 3. SCAPE distributions in case studies of mature extratropical cyclones are presented and synthesized in a schematic in Section 4. Multi-year seasonal climatologies of the CAPE and SCAPE metrics for the North Atlantic and western Europe followed by results of their correlation against precipitation (for this region) are presented in Sections 5 and 6. The climatology of the VRS instability and its correlation against precipitation are presented in Section 7. A discussion and some conclusions are given in Sections 8 and 9, respectively.

2. Methods

2.1. ERA-Interim

Climatologies and case studies of CSI presented in this paper are conducted using data from the ERA-Interim re-analysis dataset. ERA-Interim is an archive of re-analyses and short-range forecasts produced by the European Centre for Medium-Range Weather Forecasts (ECMWF), providing a wide range of meteorological data at 6-hourly intervals from 0000 UTC 1 January 1979 until the present. The data used here is from January 1979 to December 2010. The horizontal grid spacing of ERA-Interim is ~80 km (T255) and the data used has been interpolated onto a Gaussian grid with a uniform longitudinal grid spacing of 0.7° and similar (but non-uniform) latitudinal grid spacing. The forecast model used in ERA-Interim was adapted from version Cy31r1 of the Integrated Forecasting System (IFS) used operationally by ECMWF between 12 September 2006 and 2 June 2008. An overview of the forecast model, data assimilation method and input datasets is described by Dee et al. (2011), while Berrisford et al. (2009) provide a technical documentation of the available data.

2.2. CAPE calculation

Pseudo-adiabatic CAPE is defined as the kinetic energy that a parcel would gain if lifted pseudo-adiabatically from its level of free convection (LFC) to its level of neutral buoyancy (LNB):

$$\mathrm{CAPE} = \int_{p_{LFC}}^{p_{LNB}} R_d(T_{v,par} - T_{v,env}) d\ln(p), \tag{1}$$

where p_{LFC} and p_{LNB} are the pressures at the LFC and LNB respectively, R_d is the gas constant for dry air and $T_{v,par}$ and $T_{v,env}$ are the virtual temperatures of the parcel and environment respectively (Emanuel, 1994). Pseudo-adiabatic lifting means that any condensed water is assumed to rain out immediately.

CAPE was calculated using the pseudo-adiabatic CAPE code provided by Kerry Emanuel[2] , with minor modifications to include the assumptions and definitions mentioned in this section. Due to the turbulent nature of the convective boundary layer, ideally multiple CAPE values would be calculated from successive parcels launched at regular height or pressure intervals within the boundary layer (or even throughout the whole troposphere) and the maximum value of CAPE from these launches reported as the value of CAPE for that profile. To reduce the computational expense of producing a 32-year climatology of CAPE or SCAPE from 6-hourly data, the CAPE used here is calculated from a single parcel ascent, launched from the first pressure level above the surface. The impact of the different approaches was assessed by comparing the CAPE calculated over the domain shown in Fig. 1 for the month of November 2009 (not shown). Although the quantitative values were slightly different on a grid-point by grid-point basis, the location and typical values of the CAPE features relative to the extratropical cyclones and the precipitation bands were very similar.

2.3. SCAPE calculation

SCAPE was calculated as the CAPE along a sloping trajectory that is the intersection along surfaces of constant horizontal pseudo-angular momentum orthogonal components, $M = fx + v$ and $N = fy - u$, rather than along a vertical ascent (following Shutts, 1990b, and Gray and Thorpe, 2001). Here f is the Coriolis parameter calculated at the base of the ascent, u and v are wind velocities in the x and y direction respectively, and the x and y axes are aligned along lines of longitude and latitude respectively (Emanuel, 1994). There are arguments for using both the geostrophic and full winds when considering momentum surfaces and the derivation of saturated MPV: although usually derived using geostrophic winds, some authors, e.g. Gray and Thorpe (2001), argue for the use of the full winds based on both practical (geostrophic winds derived from high-resolution model output are often noisy) and theoretical grounds. Here we use the full wind in the calculation of both the SCAPE and the VRS instability. Although Gray and Thorpe (2001) derive a more accurate calculation of SCAPE following parcel trajectories, the standard SCAPE calculation as described by Shutts (1990b) was used here due to its lower computational expense. This parcel theory-based assessment of CSI has the advantage that it provides an indication of the energy yielded on instability release (that can then be used to infer the kinetic energy and so speed of the resultant motions). However, it does not directly indicate whether CSI is being, or will be, released and is computationally expensive to calculate. An alternative local (grid point) diagnosis for the presence of CSI release is thus described below.

2.4. VRS calculation

Schultz and Schumacher (1999) recommend that the release of CSI should be assessed by checking whether the three ingredients of instability, moisture and lift are present. CSI is diagnosed as existing when there is negative saturated MPV, conditional stability (positive saturated moist static stability) and inertial stability (positive absolute vorticity). Moisture is assessed as sufficient when relative humidity exceeds a threshold and the criterion of lift is simply satisfied when there is upward motion. Schultz and Schumacher's recommendation led Dixon et al. (2002) to develop the VRS instability diagnostic: a diagnosis of the number of model levels in each column where those three ingredients are present (strictly Dixon et al. (2002) used geostrophic MPV rather than the saturated MPV used here). The same VRS instability diagnostic was used by Morcrette (2004) who presented maps of CAPE, SCAPE and VRS instability for a number of case studies around the UK. In this study, the VRS instability diagnostic is modified slightly to report the total depth, in kilometres, over which the three ingredients are present. The ERA-Interim grid spacing is too coarse to adequately simulate CSI release, so a region where VRS instability is greater than zero is interpreted as representing regions where CSI release could take place in the real atmosphere, or where CSI release could be simulated if a model with high enough resolution was used. In summary, we view VRS > 0 km as indicative of CSI release.

A relative humidity threshold of less than 100% is used in the VRS instability diagnostic by analogy with cloud parametrization schemes used by global numerical models which typically allow cloud to form before the grid-box-mean relative humidity reaches 100% to account for sub-grid scale humidity fluctuations (e.g. Smith, 1990). Relative humidity thresholds between 80 and 100% were investigated by Glinton (2013). The use of 80% leads to wide-spread areas of VRS instability around extratropical cyclones, while increasing the threshold leads to progressively tighter features. Here, a relative humidity threshold of 95% is used as in Dixon et al. (2002).

3. Correlation of observed precipitation with CAPE and SCAPE over the United Kingdom

In this section, observations of daily-accumulated precipitation are compared to daily-averaged CAPE and SCAPE. The precipitation measurements are for the UK (including data from England, Wales, Scotland and Northern Ireland) and are taken from the HadUKP dataset produced by Alexander and Jones (2001). These daily-accumulated precipitation values, spanning 09 to 09 UTC and from around 86 spatially-homogeneous rain gauges across the UK, were averaged to form a single UK-wide daily-mean precipitation value. This was done for each day in the period spanning January 1979 to December 2010. Corresponding approximate daily-averaged SCAPE and CAPE values for the period 09 to 09 UTC were calculated by taking the mean of distributions derived from ERA-Interim analyses at 12, 18, 00 and 06 UTC. Average UK values were taken from the mean of values from all the ERA-Interim grid points over the UK inferred using the ERA-Interim land-sea mask. The advantage of comparing data valid over 24-hour periods on the relatively large spatial scale of the UK is that it removes noise due to precipitation typically occurring downstream of where the instability index is maximum. Previous work has shown that correlations exist between CAPE and precipitation (e.g. Monkam, 2002, Subrahmanyam et al., 2015, Zawadzi et al., 1981), especially when the comparisons are made over a sufficiently large spatial area and time period, rather than for an individual site and precipitation event.

Table 1 summarises the correlations between observed UK-average daily-accumulated precipitation and the UK-average daily-mean CAPE and SCAPE. As well as correlating the precipitation with the stability indices for the same time period, correlation coefficients were also calculated for the accumulated precipitation occurring 24 h after the period for which the stability indices are valid. Two different correlation coefficients are also shown (the Pearson product-moment and Spearman's rank). Values of the Spearman rank correlation coefficients have larger values than the corresponding Pearson product-moment correlation coefficients. Two key differences between the correlation coefficients exist. First, the Spearman coefficient is more suited to measuring non-linear relationships and will give a value of 1 when there is a perfect monotonic relationship; in contrast, the Pearson coefficient will always be less than one for perfect monotonic non-linear relationships. Second, the Pearson coefficient is more sensitive to extreme values. The main reason that the Spearman correlations are greater than the Pearson correlations

[2] Available from http://wind.mit.edu/~emanuel/ftpacc.html. Downloaded in October 2009.

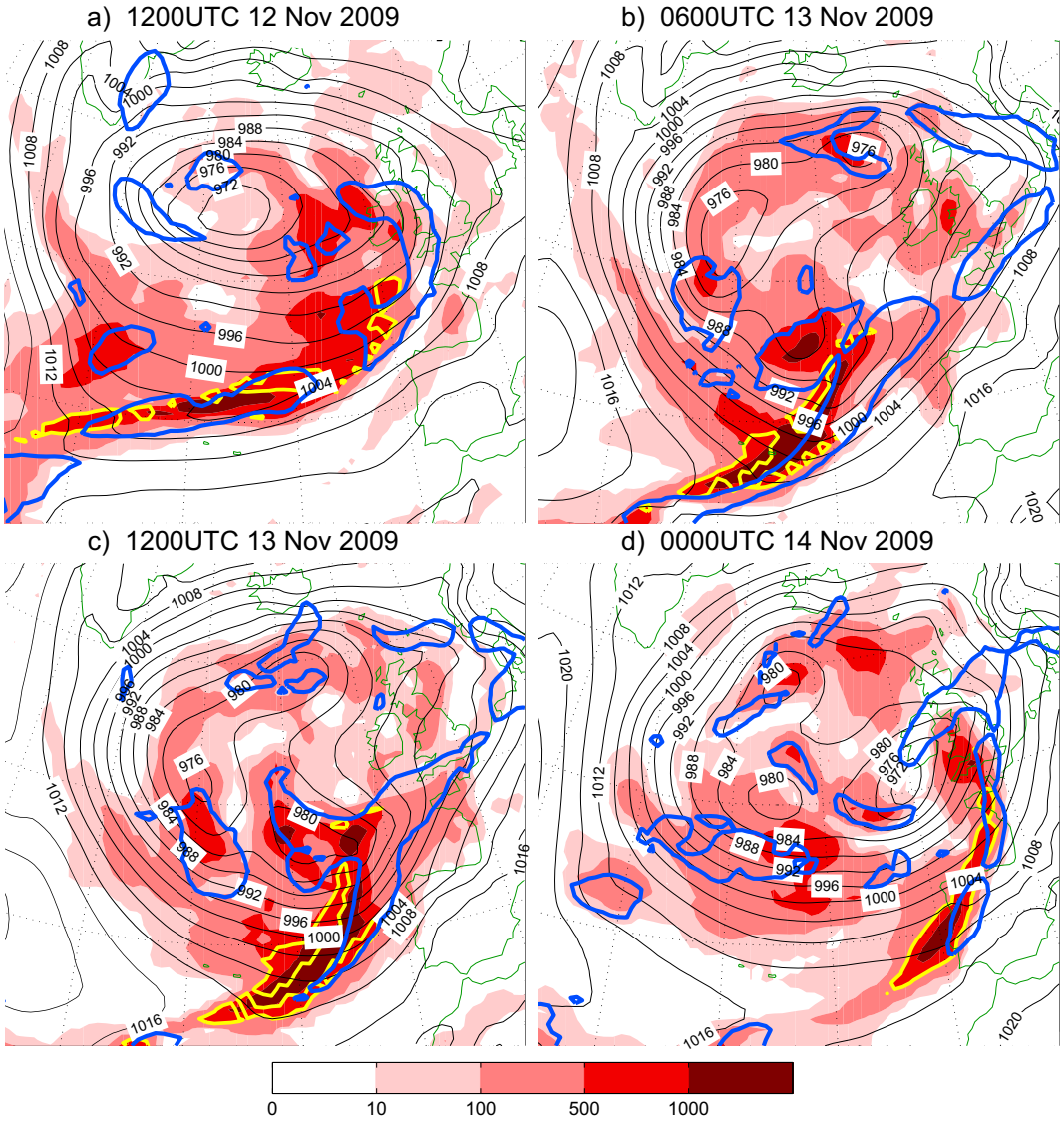

Fig. 1. SCAPE (J kg^{-1}) shaded red, ERA-Interim accumulated forecast precipitation of 1.5 mm during a 3 h accumulation period following the specified times contoured blue (see Section 2.1 for details), the yellow contour bounds SCAPE$>$ 500 J kg^{-1} where CAPE$<$ 100 J kg^{-1} and mean sea level pressure (hPa) is contoured black. (For interpretation of the references to color in this figure legend, the reader is referred to the web version of this article.)

is that the association between CAPE or SCAPE and precipitation is stronger for low values and weaker for extreme values i.e. if there is some CAPE or SCAPE then there is likely to be some precipitation, but larger values of CAPE or SCAPE are only weakly associated with larger values of precipitation.

The correlation coefficients in Table 1 are all substantially less than unity. This is expected because midlatitude processes such as large-scale ascent in the warm conveyor belts of extratropical cyclones and orographic enhancement generate stratiform cloud which precipitates, but is not generated by the release of convective instability. The question of interest here is thus not what the individual correlations are (which is difficult to interpret), but instead whether (and by how much) SCAPE correlates with precipitation better than CAPE. Table 1 shows that irrespective of which correlation coefficient is used, there is a higher correlation between UK-wide precipitation and SCAPE than there is between UK-wide precipitation and CAPE. Additionally, the higher correlation is found whether the index is compared to the precipitation accumulation over the same day or over the subsequent day.

The difference between SCAPE and CAPE is that while CAPE is calculated following a vertical trajectory, SCAPE is calculated along a surface of constant absolute momentum. The higher correlation coefficients found when comparing precipitation with SCAPE than with CAPE suggests that a significant portion of the precipitation in the UK is associated with mid-latitude baroclinic systems, which have tilted absolute momentum surfaces. It also suggests that there is some

Table 1
Correlation coefficients over the UK between 24-hour accumulated observed precipitation and model-inferred 24-hour average measures of atmospheric stability. Correlations are calculated between stability indices and observed precipitation valid for the same 24-hour period and for precipitation valid over the subsequent 24-hour period.

	CAPE		SCAPE	
	Pearson	Spearman	Pearson	Spearman
0 h offset	0.21	0.31	0.43	0.50
24 h offset	0.11	0.16	0.27	0.32

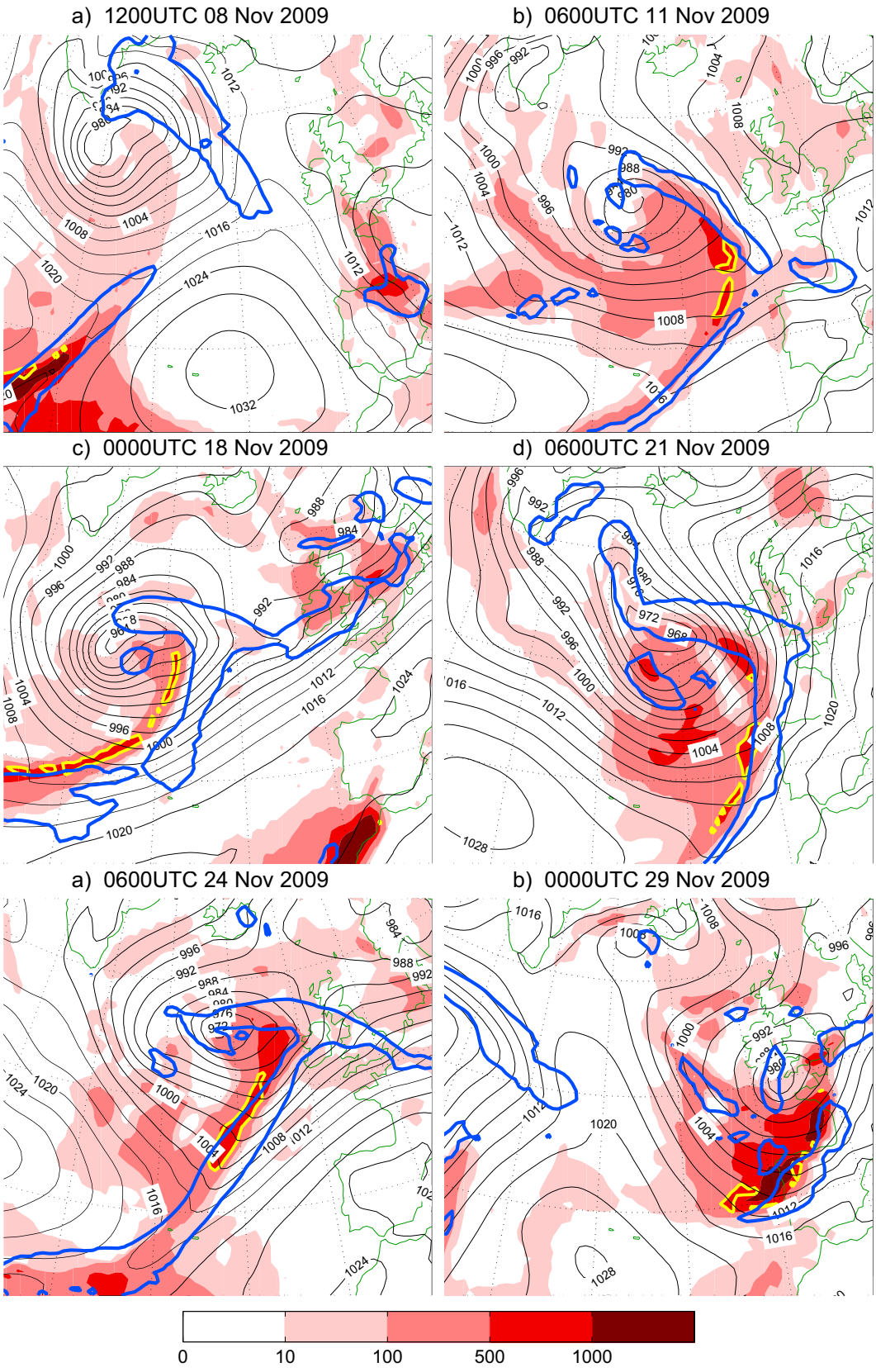

Fig. 2. SCAPE (J kg^{-1}) shaded red, ERA-Interim accumulated forecast precipitation of 1.5 mm per 3 h accumulation period contoured blue (see Section 2.1 for details), the yellow contour bounds SCAPE $>$ 500 J kg^{-1} where CAPE $<$ 100 J kg^{-1} and mean sea level pressure (hPa) is contoured black. (For interpretation of the references to color in this figure legend, the reader is referred to the web version of this article.)

potentially useful information contained within a convective instability metric when that metric includes the possibility of slantwise ascent. Although it is not surprising to find that slantwise instability within baroclinic systems is contributing to precipitation in the UK, this effect has not been previously quantified. This finding, determined over the relatively small UK area using observed precipitation data, motivates the rest of this paper. The locations where SCAPE exists within an extratropical cyclone and their relationship to the locations of precipitation features are now determined.

4. Distributions of CAPE and SCAPE in extratropical cyclones

Maps of CAPE and SCAPE calculated from ERA-Interim data were plotted at six-hourly intervals throughout November 2009 to select case studies for further analysis. This month was chosen because it was an active month in terms of extratropical cyclones in the North Atlantic. Fig. 1 shows maps of SCAPE and mean-sea-level pressure for a case study from the 12–14 November 2009. This frontal-wave cyclone passed over the UK in its mature phase on the evening of 13 November 2009 bringing strong surface winds and intense precipitation. Emanuel (1983) gives the time scales for conditional instability (CI) and conditional symmetric instability (CSI) release as the inverse Brunt-Väisälä frequency (typically around 30 min) and the inverse Coriolis parameter (typically 4 to 6 h in the mid-latitudes), respectively. As a result, if CSI co-exists alongside CI then the release of CI is expected to dominate. However, places where CSI exists and where CI is small might be expected to exhibit circulations associated with CSI release (in the real atmosphere or in models with sufficient resolution). These regions exist where SCAPE is large while CAPE is small (objectively defined as SCAPE $> 500\ \mathrm{J\ kg^{-1}}$ and CAPE $< 100\ \mathrm{J\ kg^{-1}}$ and enclosed by yellow contours in Figs. 1 and 2); we term these 'potential CSI release regions'. While necessarily somewhat arbitrary, the values for the SCAPE and CAPE thresholds were chosen based on both the pre-existing literature and preliminary analysis of the data. Shutts (1990b) found that three of the five explosive cyclogenesis cases he studied had regions where SCAPE $> 1000\ \mathrm{J\ kg^{-1}}$ and CAPE $< 100\ \mathrm{J\ kg^{-1}}$. Considering more typical winter cyclones, examination of the 13 North Atlantic cyclones that occurred during November 2009 found that more than half of them had at least one potential CSI release region according to the thresholds chosen above (not shown). Other studies have identified SCAPE release for even smaller values of SCAPE (e.g. Browning et al. (2001) present stacked slantwise convective circulations, attributed to SCAPE release, in a cold front over the UK where SCAPE just exceeds $>100\ \mathrm{J\ kg^{-1}}$). Hence, while there will likely be some sensitivity to the precise threshold chosen, these thresholds provide a realistic guide to potential CSI release in cyclones.

The formation of the cyclone in Fig. 1 can be tracked from a mean-sea-level pressure trough that formed to the southwest of a pre-existing large-scale low pressure system, visible at 1200 UTC on 12 November at about 45°N, 40°W (Fig. 1a). The trough was associated with a precipitation band that moved towards a preexisting cold frontal precipitation band. By 0600 UTC on 13 November (Fig. 1b), the precipitation band associated with the trough was almost joined to the cold frontal precipitation band; hence the formation of this cyclone can be described as an instant occlusion process (Bader et al., 1995). Potential CSI release regions are sandwiched between the trough's precipitation band and the cold frontal precipitation band. Six hours later at 1200 UTC (Fig. 1c), the trough's precipitation band had fully merged with the cold frontal precipitation band completing the instant occlusion process. At 0000 UTC on 14 November (Fig. 1d) the frontal wave was in its mature phase, when it brought strong surface winds to the UK (not shown).

The association of cold fronts with potential CSI release regions is common in mature extratropical cyclones as illustrated by the further examples presented in Fig. 2. These 6 cases were chosen from the 13 North Atlantic cyclones that occurred during November 2009 to represent those that were most likely to have had CSI release, judged from a preliminary assessment of the SCAPE distributions.

Synthesis of the findings in Figs. 1 and 2, and other SCAPE distributions from case studies described in the published literature, yields the following three common features of a mature North Atlantic extratropical cyclone:

1. large values of SCAPE along the cold front, including potential CSI release regions,
2. an absence of SCAPE along the warm front, and
3. a region of moderately large SCAPE values (up to $\sim 500\ \mathrm{J\ kg^{-1}}$) in the cold sector where CAPE has similar magnitude and hence the release of CI is more likely than the release of CSI.

These features are presented schematically in Fig. 3 and are described in more detail below with reference to the case studies shown in Figs. 1 and 2. The purpose of this schematic is to illustrate the typical distributions of CAPE and SCAPE and so aid in the interpretation of the climatologies presented in Section 5.

All six examples in Fig. 2 have at least one potential CSI release region close to the cold front. These regions tend to be on the cold side of the cold frontal precipitation band and Fig. 2c shows the most extreme example, with a potential CSI release region that is so far on the cold side of the cold frontal rainband that is does not overlap with it. Other studies have also reported large SCAPE values in the vicinity of cold fronts. Sheldon (2015) composited cross-sections of SCAPE along cold fronts and found that the (composited) maximum of cross-frontal SCAPE is co-located with the surface cold-frontal boundary. Gray et al. (2011) show SCAPE and CAPE distributions for four North Atlantic cyclones and show large values of SCAPE (up to $700\ \mathrm{J\ kg^{-1}}$ for parcels lifted from near the ground) coinciding with much smaller values of CAPE (less than $300\ \mathrm{J\ kg^{-1}}$) found behind the cold-frontal cloud band in those cases. Browning et al. (2001) diagnosed slantwise circulations from radar velocity measurements, and calculated SCAPE to assess the role of CSI. They found the largest SCAPE values were along the cold front, though they were relatively small (reaching between 100 and $300\ \mathrm{J\ kg^{-1}}$).

In all six examples in Fig. 2, warm frontal precipitation bands are generally associated with small or negligible values of SCAPE.

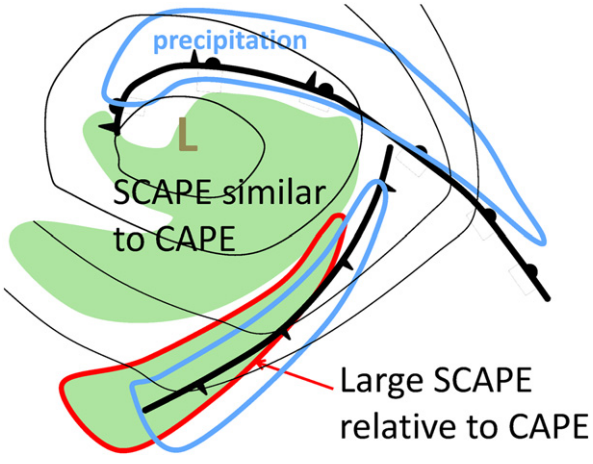

Fig. 3. A schematic of the typical location of SCAPE and CAPE features with relative to the frontal precipitation bands in an extratropical low pressure system (labelled "L"). The cold, warm and occluded fronts are shown with thick black lines and mean-level-pressure using thin black lines. Large-scale frontal precipitation bands are shown by the blue contour. Non-zero SCAPE is shaded green and locations where SCAPE $> 500\ \mathrm{J\ kg^{-1}}$ and CAPE $< 100\ \mathrm{J\ kg^{-1}}$ are contoured in red. (For interpretation of the references to color in this figure legend, the reader is referred to the web version of this article.)

These examples are taken from mature extratropical cyclones, but from inspecting all six-hourly SCAPE charts in November 2009 it was found that warm fronts in all stages of their life cycles generally had little or no SCAPE. The 13 November case study presented in Fig. 1 is unusual in that it did have large values of SCAPE ($>500\ J\ kg^{-1}$); this was because the warm front developed as part of a frontal-wave structure where large SCAPE was present prior to the cyclone development. A possible reason for small values of SCAPE along the warm front is given by Gray and Thorpe (2001) who found in a case study that more SCAPE was diagnosed along the warm front when the assumption of axisymmetric, non-evolving flow was abandoned in the SCAPE calculation. The authors compared SCAPE calculated according to Shutts (1990b), which assumed a geostrophic non-evolving axisymmetric flow, with SCAPE calculated using both model trajectories and "non-rapid" trajectories for which the axisymmetric assumption was removed by advecting air parcels with the resolved winds as they ascended the momentum surface. It is not computationally feasible to perform the non-rapid or model trajectory calculations in this climatological dataset. Thus it is possible that SCAPE in warm sectors has been under-estimated in these case studies.

All examples in Figs. 1 and 2 show a broad region of SCAPE in the cold sector behind the cold front where SCAPE is comparable to CAPE. Further analysis of the SCAPE and CAPE values (not shown) revealed this region usually had SCAPE values around 1.5 times the associated CAPE values. These relatively large CAPE values suggest that the release of CI is more likely than the release of CSI here. Observational evidence for CI release in the cold sector of cyclones is the cumulus convection cells often seen there in satellite imagery.

The typical SCAPE distribution described here along the cold front, warm front and in the cold sector is consistent across the cases examined here and in the literature. However, there is less agreement on the SCAPE typically found in the cloud head of mature cyclones. The SCAPE distributions shown for the cases studied by Shutts (1990b), Shutts (1990a), Gray and Thorpe (2001) and Dixon et al. (2002) differ from those presented here in that they have large values of SCAPE collocated with a developing cloud head. Those cases were for a particular class of rapidly-developing extratropical cyclone in which a convex cloud head develops and can be associated with CSI release. However, Gray et al. (2011) found broad regions where SCAPE exceeded $300\ J\ kg^{-1}$ (for parcels lifted from

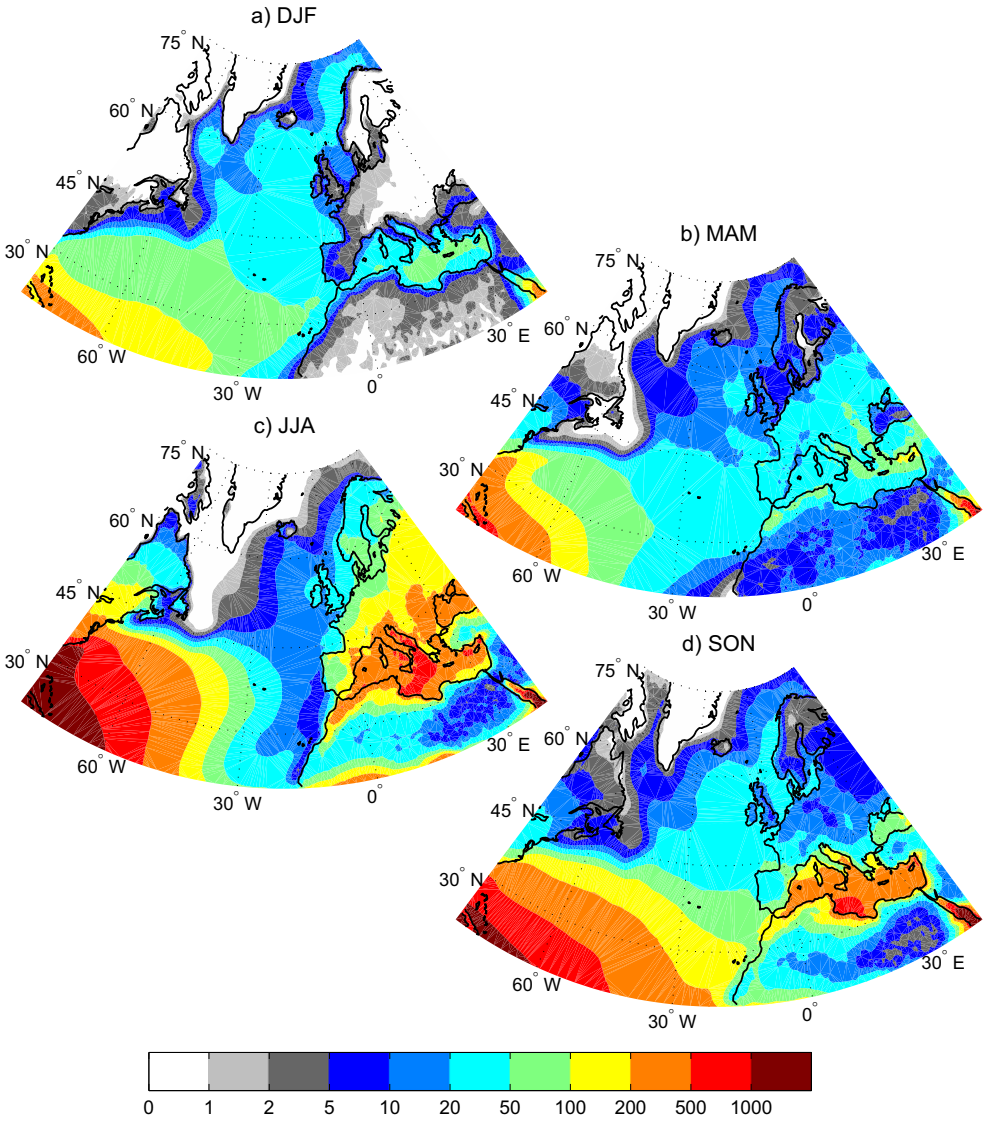

Fig. 4. Mean CAPE ($J\ kg^{-1}$) for a) DJF, b) MAM, c) JJA and d) SON for 1979–2010.

near the surface) in only one of the four cases of rapidly-developing extratropical cyclones that they analysed.

5. Climatology of CAPE and SCAPE instability indices

The ultimate goal of this paper is to quantify the role that slantwise convection may have in modulating the distribution of precipitation on the mesoscale by producing a climatology of VRS instability and correlating it to surface precipitation. For the purposes of comparison with the VRS instability climatology, a climatology of SCAPE is first produced. However, since that itself is novel, a climatology of CAPE is also produced for comparison (given the similarity of the diagnostic design with that of SCAPE) and to demonstrate consistency with previously published literature.

5.1. CAPE climatology

The seasonal mean CAPE calculated from ERA-Interim data is shown in Fig. 4. Climatologies of CAPE have already been presented by Holley et al. (2014) for the UK, Romero et al. (2007) for Europe, Subrahmanyam et al. (2015) for India, Meukaleuni et al. (2016) for West Africa and by Riemann-Campe et al. (2009) for the globe. The CAPE climatology presented here is only briefly discussed as its main purpose is to be a reference against which the SCAPE climatology can be compared. The climatology of mean CAPE is informative, but CAPE values are often zero and the mean value of a positive variable is a product of the fractional occurrence of non-zero values and the mean of the non-zero values. These two factors are here referred to as the frequency of occurrence (FOO) and the amount when present (AWP). The climatology of FOO and AWP of CAPE are shown for the summer (June, July, August: JJA) and winter (December, January, February: DJF) seasons in Fig. 5.

Mean CAPE is closely dependent on the surface temperature and humidity conditions, relative to the tropospheric temperatures above. This is seen in winter when there is moderate mean CAPE over most the ocean (around 20–100 J kg^{-1}) and negligible mean CAPE over land (Fig. 4a). The breakdown of the mean CAPE into its FOO (Fig. 5a) and AWP (Fig. 5b) factors shows that non-zero oceanic

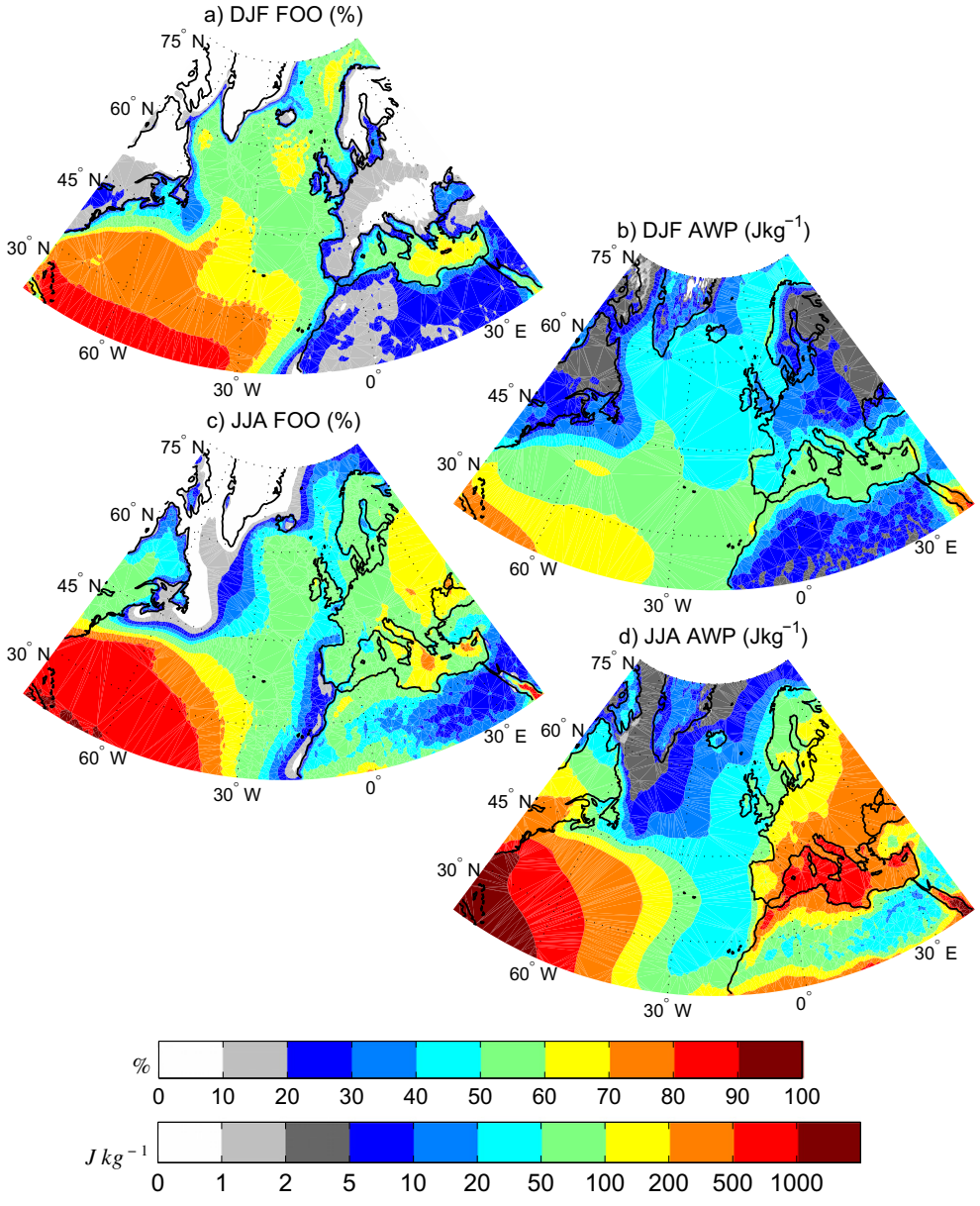

Fig. 5. (a, c) Frequency of occurrence (FOO, %) of CAPE > 0 J kg^{-1} and (b, d) mean amount when present (AWP, average CAPE when CAPE > 0 J kg^{-1}) for (a, b) DJF and (c, d) JJA.

CAPE in winter occurs frequently (mostly between 50% and 60% of the time), but with moderate amounts (AWP around 50–200 J kg^{-1}). An example of the extra information given by the breakdown of the mean CAPE into its FOO and AWP factors is given by comparing the North Sea and Portuguese regions. Although the mean CAPE values of between 5–10 J kg^{-1} are similar in these two regions, over the North Sea there is a FOO of 40–60% and an AWP of 20–50 J kg^{-1} whereas over the western coast of Portugal FOO is 20–30% and AWP is 50–100 J kg^{-1}. This implies less frequent instability, but more unstable events when instability exists, over Portugal.

From spring (March, April, May: MAM) through to summer CAPE increases over land (Figs. 4b and c). Larger values of mean CAPE (200–500 J kg^{-1}) are found around southern Europe and near the Mediterranean. The Mediterranean holds its heat well into the autumn (September, October, November: SON) when the mean CAPE is large as cooler air overruns relatively warmer waters (Fig. 4d). By far the largest FOO of CAPE (80–90%; Fig. 5c) occurs in the south-west North Atlantic at the borders of the Caribbean during summer. This is also where the largest AWP of CAPE (over 1000 J kg^{-1}) is found. This region provides another example of the extra information given by the breakdown of the mean CAPE into its FOO and AWP factors. The region of the mid-Atlantic around 45°W 35°N has a similar mean CAPE in summer to the region of the Mediterranean near Corsica and Sicily. However, in the mid-Atlantic, this mean value is due to a FOO of 70–80% and an AWP of 200 J kg^{-1} whereas over Corsica and Sicily, the FOO is 50–60% and the AWP is 500–1000 J kg^{-1}. This implies less frequent instability, but more unstable events when instability exists, over Corsica and Sicily.

5.2. SCAPE climatology

The seasonal mean SCAPE calculated from ERA-Interim data is shown in Fig. 6. Regions where the mean SCAPE is at least two times or at least three times as large as the mean CAPE are highlighted by black and pink contours, respectively.

On the whole, the pattern and magnitudes of the climatological distribution of SCAPE are largely similar to those of CAPE. This is particularly the case in summer (compare Figs. 6c and 4c) when large-scale horizontal temperature gradients become weaker and thermal wind balance leads to the absolute momentum surfaces being less tilted; consequently, SCAPE tends towards being equal to CAPE. In the other seasons SCAPE generally has larger values than CAPE, although the patterns are similar (compare panels a, b and d

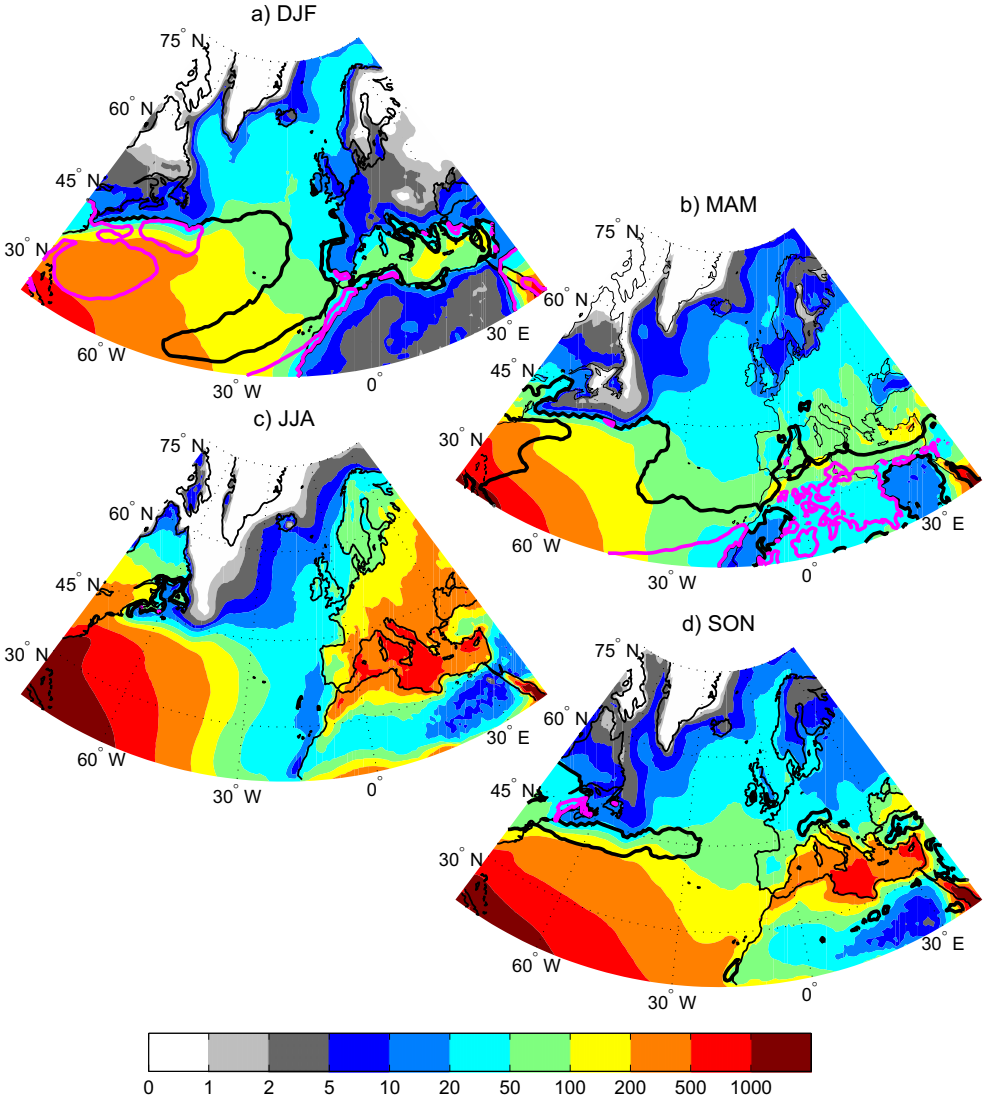

Fig. 6. Mean SCAPE (J kg^{-1}) for a) DJF, b) MAM, c) JJA and d) SON for 1979–2010. The black contour is where the ratio of mean SCAPE to mean CAPE is 2, and the pink contour is where the ratio is 3. (For interpretation of the references to color in this figure legend, the reader is referred to the web version of this article.)

in Figs. 6 and 4). The largest ratios of mean SCAPE to mean CAPE are found in winter and spring to the south of the domain shown.

In winter there is a region over the ocean near the eastern seaboard of the United States where the mean SCAPE is three times larger than the mean CAPE (Fig. 6a). The mean SCAPE here is 200–500 J kg^{-1}, whereas the mean CAPE is only 50–100 J kg^{-1} (Fig. 4a). Comparison of the FOO and AWP for both the CAPE and SCAPE in the region of the Gulf Stream shows that in general the SCAPE is larger than the CAPE as a result of having larger values of both FOO and AWP (compare Figs. 5 and 7): the FOO is 70–80% for CAPE compared to 80–90% for SCAPE and the AWP is 20–50 J kg^{-1} for CAPE compared to 100–200 J kg^{-1} for SCAPE. The subtropics are also a region of large SCAPE values (absolutely and also with respect to CAPE), particularly in winter and spring. These large values can obviously not be attributed to extratropical cyclones and are instead a consequence of the weak Coriolis effect at low latitudes. Compared with midlatitudes, an air parcel close to the equator has to travel horizontally further for adjustment to geostrophic balance for a given velocity perturbation. Hence, although temperature gradients are weak in the subtropics, momentum surfaces can have shallower slopes than those of temperature yielding large SCAPE values. A few sample cross sections of momentum surfaces showed that they did indeed be come very shallow close to the equator.

6. Correlation of model precipitation with CAPE and SCAPE over the North Atlantic and Europe

The analysis of correlations between instability metrics and observed precipitation described in Section 3 for the UK is now extended to cover the entire North Atlantic and European region using the ERA-Interim analysis for the instability metrics and ERA-Interim forecast precipitation. ERA-Interim provides 3-hour accumulated precipitation from forecasts initialised at 00 and 12 UTC, with a maximum lead time of 12 h such that they do not overlap. In this section precipitation is accumulated in the 3 h following the instance of instability, e.g. SCAPE at 06 UTC is correlated with precipitation accumulated between 06 and 09 UTC, a physically reasonable time

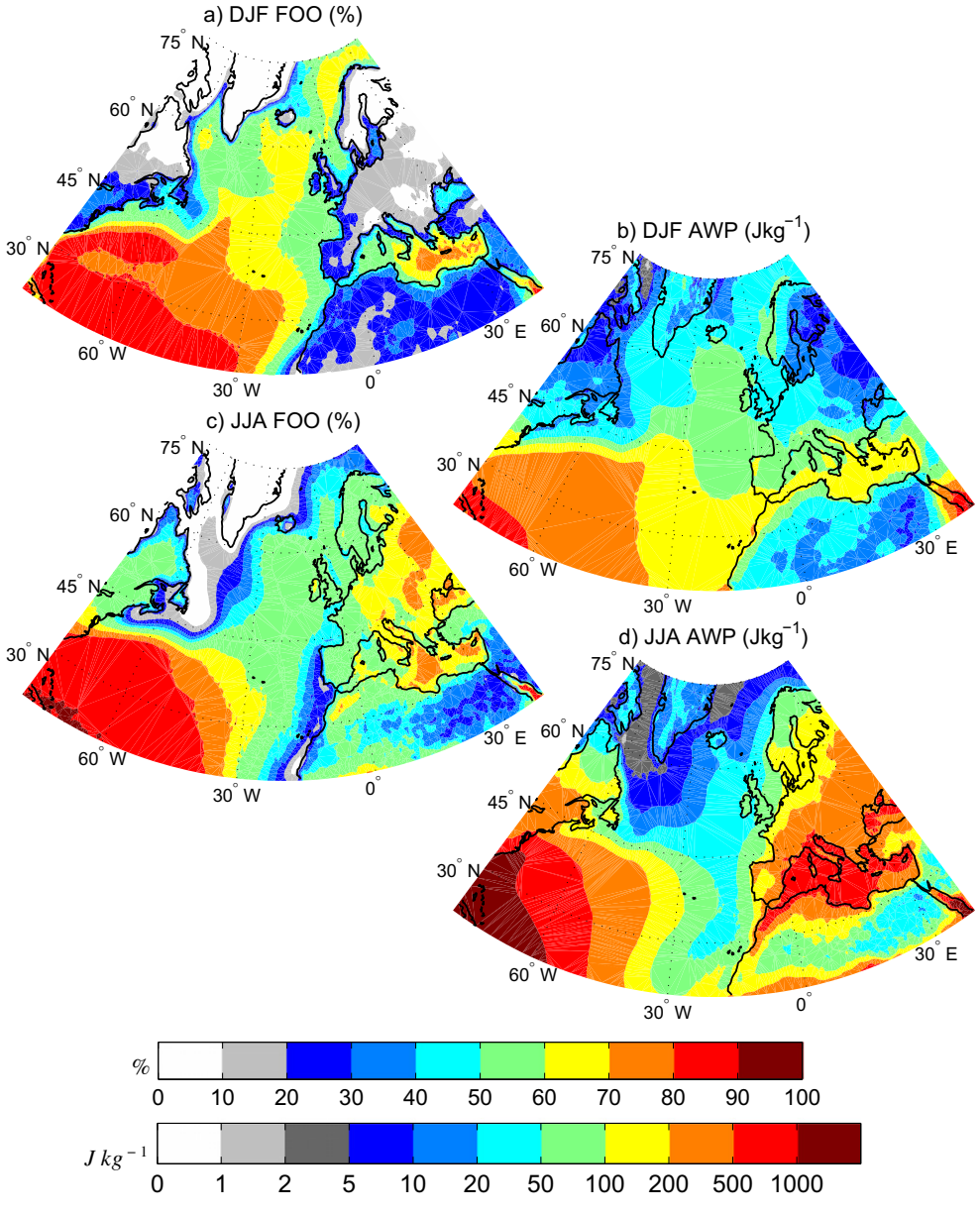

Fig. 7. (a, c) Frequency of occurrence (FOO, %) of SCAPE > 0 J kg^{-1} and (b, d) mean amount when present (AWP, average SCAPE when SCAPE > 0 J kg^{-1}) for (a, b) DJF and (c, d) JJA.

scale over which to expect precipitation manifest from CSI release. As the resolution of the model used to generate ERA-Interim is insufficient to resolve the release of CSI, it is likely that the instability is ultimately released in a non-physical way. This release may occur in the convection scheme if the CSI becomes converted to conditional instability (CI) as suggested by Gray et al. (2011). de Leeuw et al. (2014) provide a detailed comparison of ERA-Interim forecast precipitation with the England and Wales Precipitation dataset (Wigley et al., 1984) and found that the reanalysis underestimates daily precipitation amounts by 22%.

The calculation of correlation coefficients between CAPE and precipitation is mainly carried out to produce a reference against which correlations between precipitation and SCAPE can be compared. Maps of the (Pearson) correlation coefficient between CAPE and total precipitation for each of the four seasons are shown in Fig. 8. In winter, a band of relatively higher values of correlation coefficient (up to 0.7) extends across the southern North Atlantic and into the Mediterranean. Peak values are lower in the other seasons, and the region of higher values moves to the eastern North Atlantic and over Africa in the summer and autumn.

The correlation coefficient between SCAPE and total precipitation was also calculated using ERA-Interim data. Across most of the North Atlantic Gulf Stream region, extending into the mid North Atlantic, the correlation between precipitation and SCAPE is around 0.05 to 0.1 higher than between precipitation and CAPE (Fig. 9): this difference has peak values of up to 0.15 near the USA coastline in the winter, autumn and spring, but lower values the summer. The higher correlation values suggest that the SCAPE metric is quantifying aspects of the processes that modulate the distribution of precipitation that are not captured by the CAPE metric. The main exception to the generally higher correlation of SCAPE than CAPE with precipitation is over the North African coast in Winter (Fig. 9a). While interesting, the correlations may not be very reliable here due to the small amount of precipitation in this mainly desert region.

As a metric for the climatological distribution of CSI, SCAPE has the advantage that the interpretation of the resulting distribution can be easily made with reference to that of climatological distribution of CI made using CAPE. However, SCAPE is limited as a diagnostic for assessing the atmosphere's susceptibility to slantwise convection

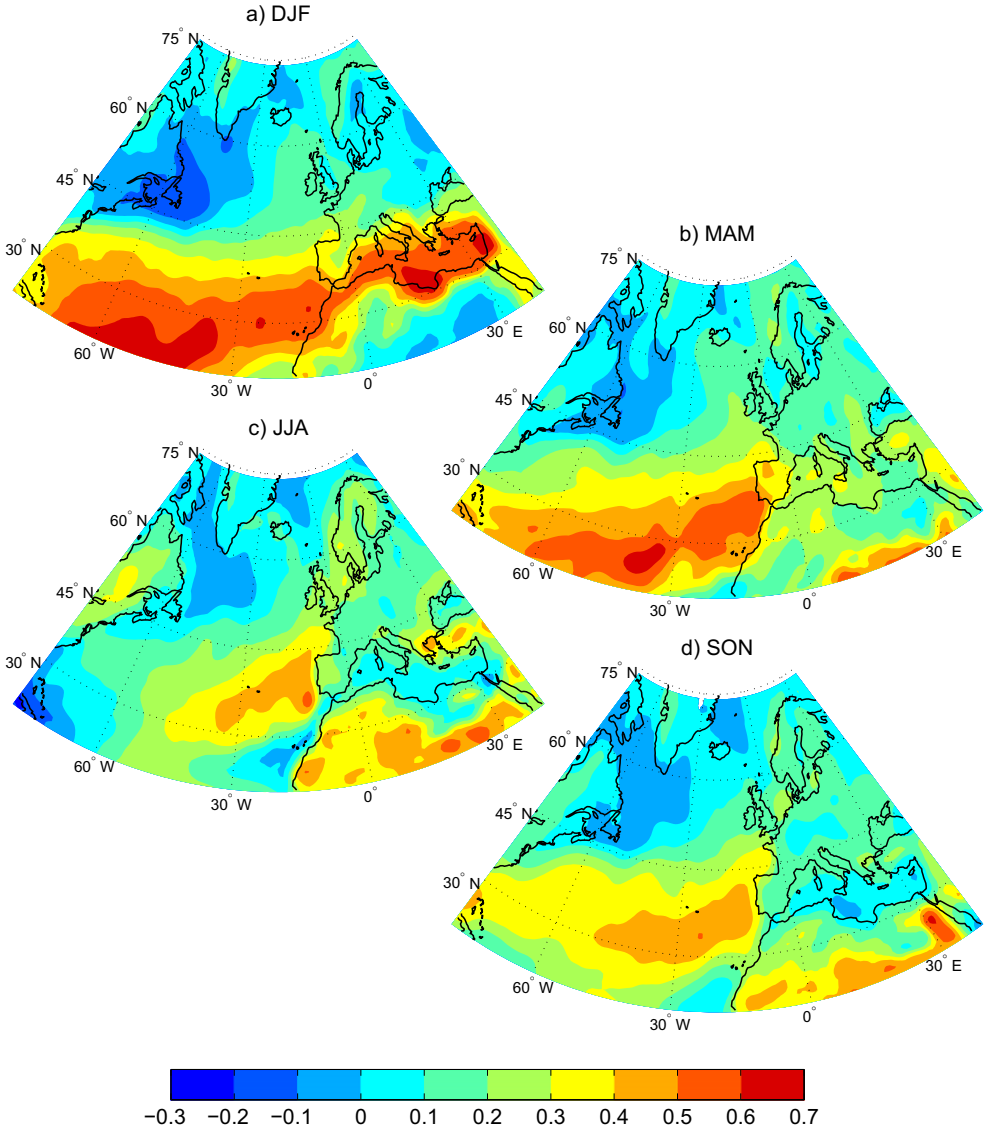

Fig. 8. Correlation (Pearson) between CAPE (at 00, 06, 12 and 18 UTC) and total accumulated precipitation over the following 3h using all data from 1979 to 2010; a) DJF, b) MAM, c) JJA and d) SON.

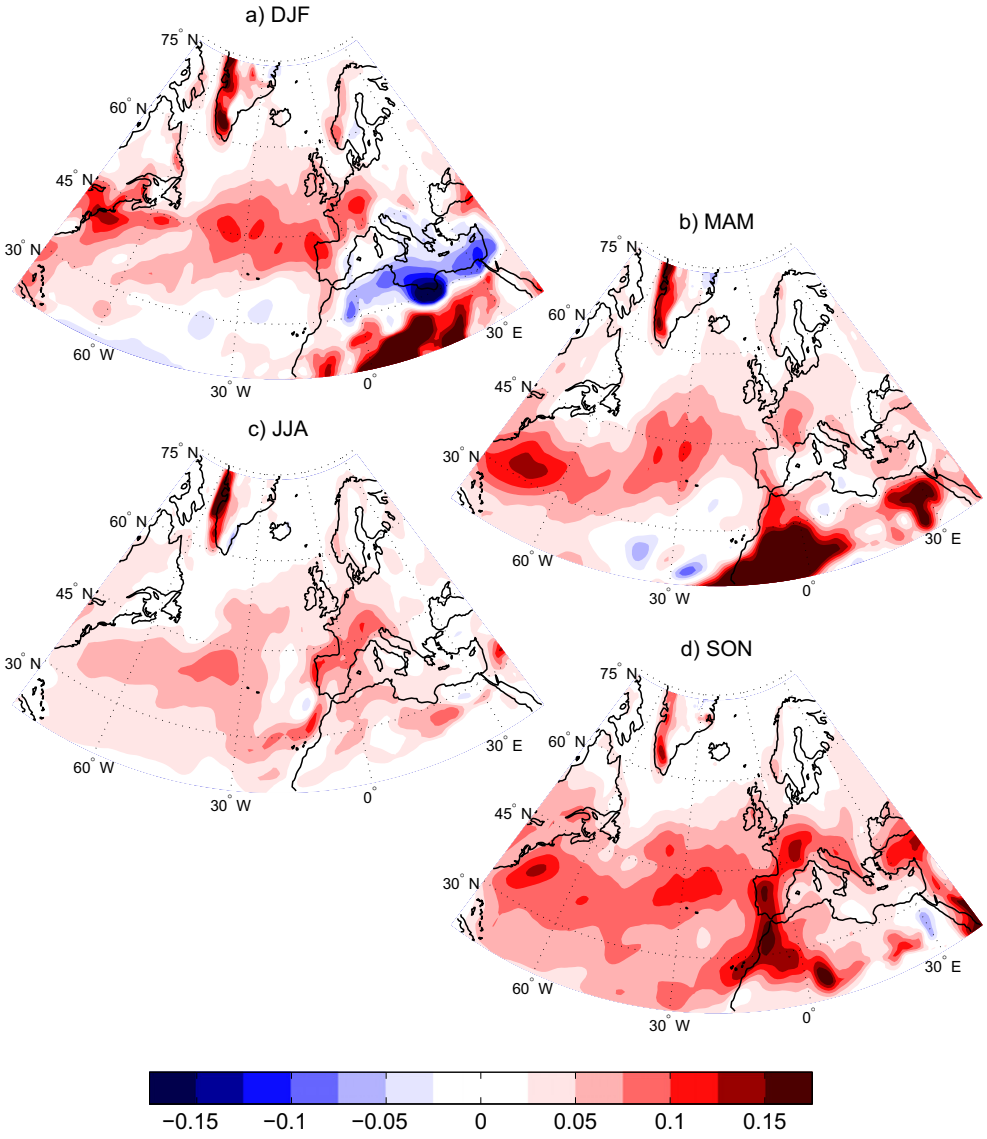

Fig. 9. Similar to Fig. 8 except it is the correlation between SCAPE and precipitation minus the correlation between CAPE and precipitation; a) DJF, b) MAM, c) JJA and d) SON.

because SCAPE, like CAPE, only quantifies the presence of the instability – there is no information about how likely the instability is to be released. Additionally, away from baroclinic regions the absolute momentum surfaces tend towards being vertical and a calculation of SCAPE is equivalent to a calculation of CAPE. A better means of assessing whether CSI release has occurred is required to quantify the potential role of CSI release in modulating the precipitation climatology.

7. VRS instability climatology and correlation with precipitation

7.1. VRS climatology

The seasonal mean VRS instability calculated from ERA-Interim data is shown in Fig. 10. A maximum in VRS that coincides with the North Atlantic storm track is particularly noticeable in the winter. Unlike the SCAPE (and CAPE) climatology, the region of peak values in the VRS climatology has a clear southern flank, with relatively small mean values equatorwards of 30°N. Mean values of the VRS instability diagnostic in the western North Atlantic are around 0.3 km, although inspection of the corresponding FOO and AWP shows that non-zero VRS instability occurs around 20% of the time and has a depth of over a km when present over a large region of the western North Atlantic gulf steam region in winter (Fig. 11a and b); the region of large AWP overlies that of large FOO, although the peak in AWP is located slightly further west. The western North Atlantic region of large FOO in summer is in a similar position to that in winter (Fig. 11c), although peak FOO values are smaller (peaking at less than 20%); peak values summer of AWP are also smaller than those in winter (Fig. 11d), peaking at about 1 km along the USA coastline in this region, further north than the peak in FOO.

7.2. Correlation of VRS with precipitation

The Pearson correlation coefficient between VRS and total precipitation, both calculated from ERA-Interim data, is shown in Fig. 12. A thick black contour highlights the regions where the correlation is larger between VRS instability and precipitation than between SCAPE and precipitation (and where that correlation is larger than 0.4 and hence not trivially small). Large portions of the North Atlantic storm track have correlations between VRS instability and precipitation exceeding 0.5. Although correlations exceeding 0.5 do not mean that VRS instability is a perfect predictor of the location and intensity of

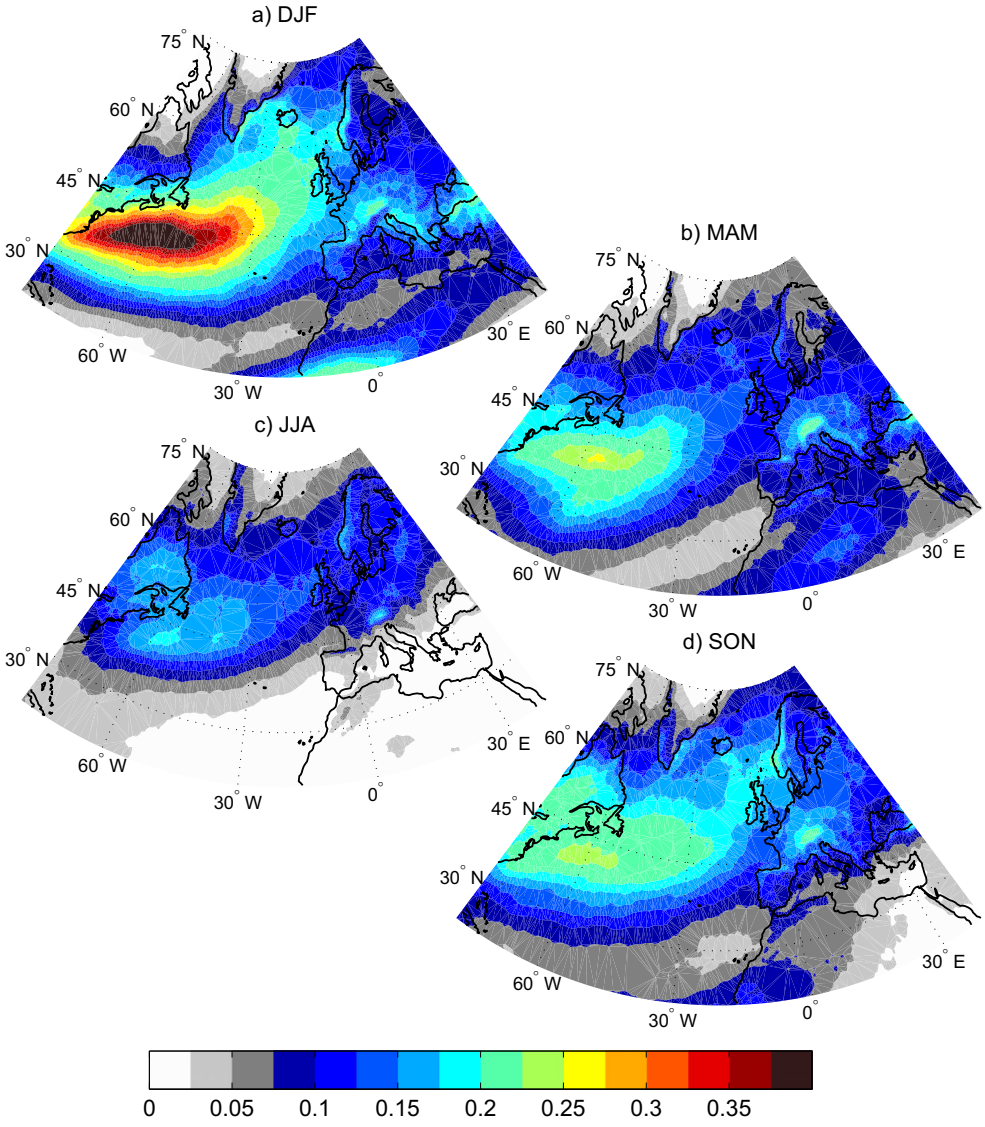

Fig. 10. Mean VRS (km) for a) DJF, b) MAM, c) JJA and d) SON, for 1979–2010.

precipitation, they do suggest that the diagnostic encapsulates something about the atmospheric flow and its thermodynamic structure that quantifies the prevalence of regions susceptible to CSI that then lead to a detectable signal in terms of precipitation patterns.

8. Discussion

Bennetts and Hoskins (1979) suggested that CSI release may be one of the mechanisms responsible for frontal precipitation forming into bands and hence modulating the intensity and accumulation of precipitation at the surface on the mesoscale. Since the release of CSI requires the presence of a moist unstable profile along an absolute momentum surface, SCAPE was used to look for possible correlations between precipitation and slantwise instability over the North Atlantic and European region (Section 6). There is larger correlation between SCAPE and precipitation than between CAPE and precipitation over much of the North Atlantic storm track, extending into western Europe, all year around (Fig. 9).

A long time series of self-consistent meteorological data covering a large domain was required to perform this comparison. Atmospheric data from ERA-Interim was used here. Although the horizontal resolution (equivalent grid spacing ≃80 km) of ERA-Interim is too coarse to expect the model used to be accurately representing the slantwise circulations associated with the release of CSI, the model can represent the large-scale flow patterns and thermodynamic structures from which regions where CSI release ought to be occurring can be diagnosed. Gray et al. (2011) studied the evolution of regions susceptible to CSI release in a weather forecast model at two different grid spacings (about 40 and 12 km) for a number of North Atlantic storms and found regions susceptible to CSI release for both resolution configurations. By tracking the time evolution of the size of the region where conditions consistent with CSI release existed, they found a delay in the reduction of the size of this region in the coarser resolution model relative to the higher resolution one. This suggests that if a numerical weather prediction model contains a region of CSI then, over time, circulations will develop that lead to the instability being released. However, if the model resolution is too coarse to properly resolve the circulations associated with the release of the instability, then it is possible that the CSI will be released in a non-physical way. For example, the CSI could eventually be converted to CI and released through the convection scheme.

One way of interpreting the correlation between precipitation and SCAPE or VRS instability in the ERA-Interim data is that the precipitation is there due to the release of CSI. However, since both

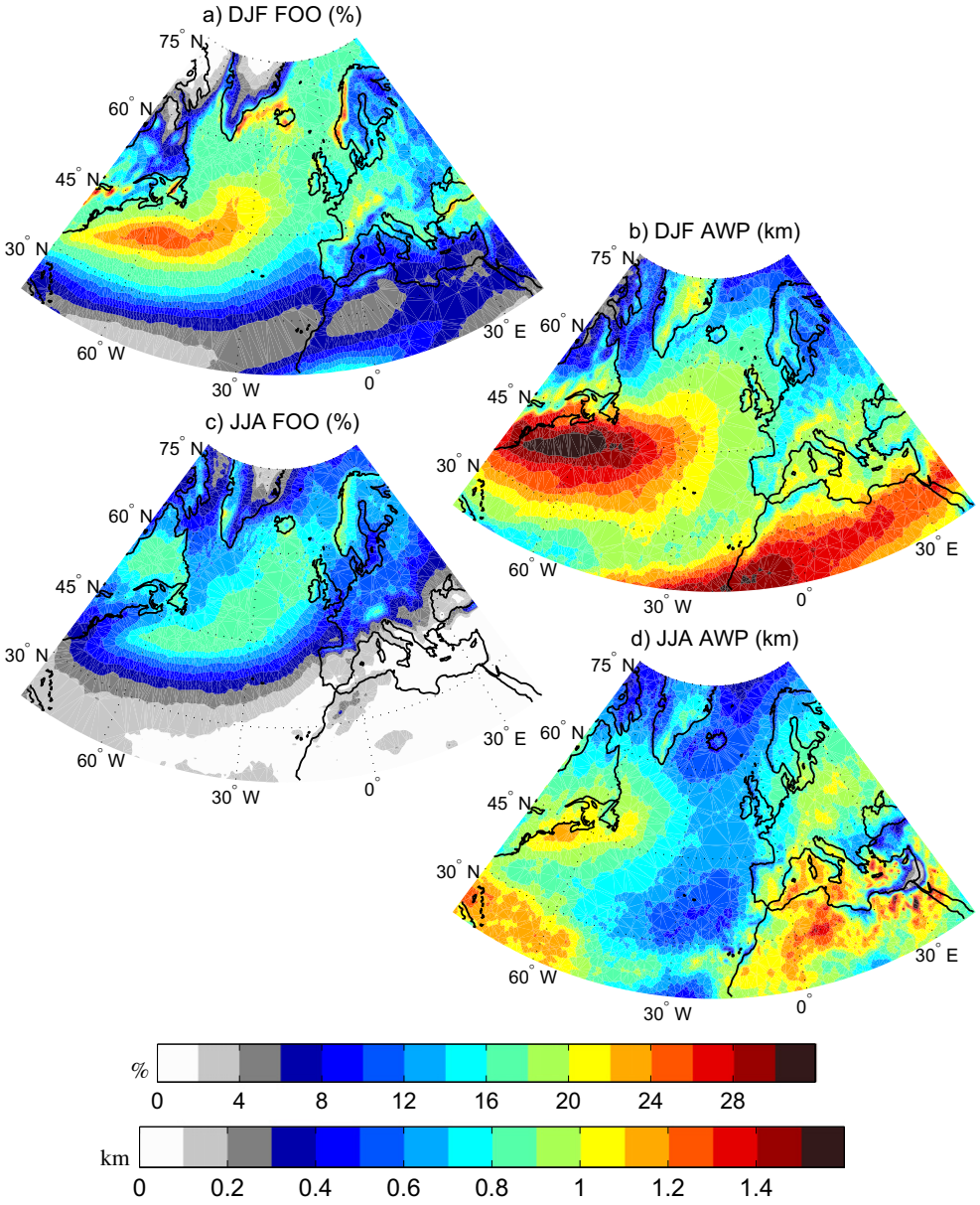

Fig. 11. (a, c) Frequency of occurrence (FOO, %) of VRS > 0 km and (b, d) mean amount when present (AWP, average VRS when VRS > 0 km) for (a, b) DJF and (c, d) JJA.

the vertical and horizontal grid in the model used to generate ERA-Interim are likely to be too coarse to allow CSI circulations to be resolved correctly, this interpretation is unlikely to be correct. An alternative paradigm is that precipitation generally occurs in regions of cyclones where CSI exists and that the correlation shown here indicates that the spatial distribution and maxima of precipitation would have been modulated in these regions if the model had been able to resolve CSI release. This potential modulation of precipitation due to CSI release raises a number of interesting questions. If a numerical model is used to predict the occurrence of extratropical cyclones and the statistical properties of surface winds or precipitation accumulation in the future, then it is important that the model is able to accurately represent all the processes that modulate surface wind speed and local precipitation distributions. The climatology of VRS instability presented here suggests that regions susceptible to CSI release are relatively common. One area for future work would be to focus on the impact that properly resolving regions of CSI may have on the distributions of precipitation on the timescale of a season and the spatial scale of a whole storm track.

If resolving regions of CSI release, and the slantwise circulations associated with them, is shown to be important for certain applications then two avenues present themselves. Either (i) slantwise parametrization schemes such as those described by Lindstrom and Nordeng (1992) or Balasubramanian and Yau (1994) should be considered, either for inclusion into the coarse resolution models or as a means of post-processing the coarse-resolution model output, or (ii) consistent with the findings of Kendon et al. (2012), the use of high horizontal and vertical resolution models should be considered for downscaling seasonal and decadal projections used in certain hydrological and wind-speed applications.

9. Conclusions

Data from 32 years of ERA-Interim and observed precipitation accumulation were used to calculate correlations between CAPE and precipitation and between SCAPE and precipitation over the UK. Correlations with SCAPE were found to be higher than with CAPE which motivated the research described in the remainder of this

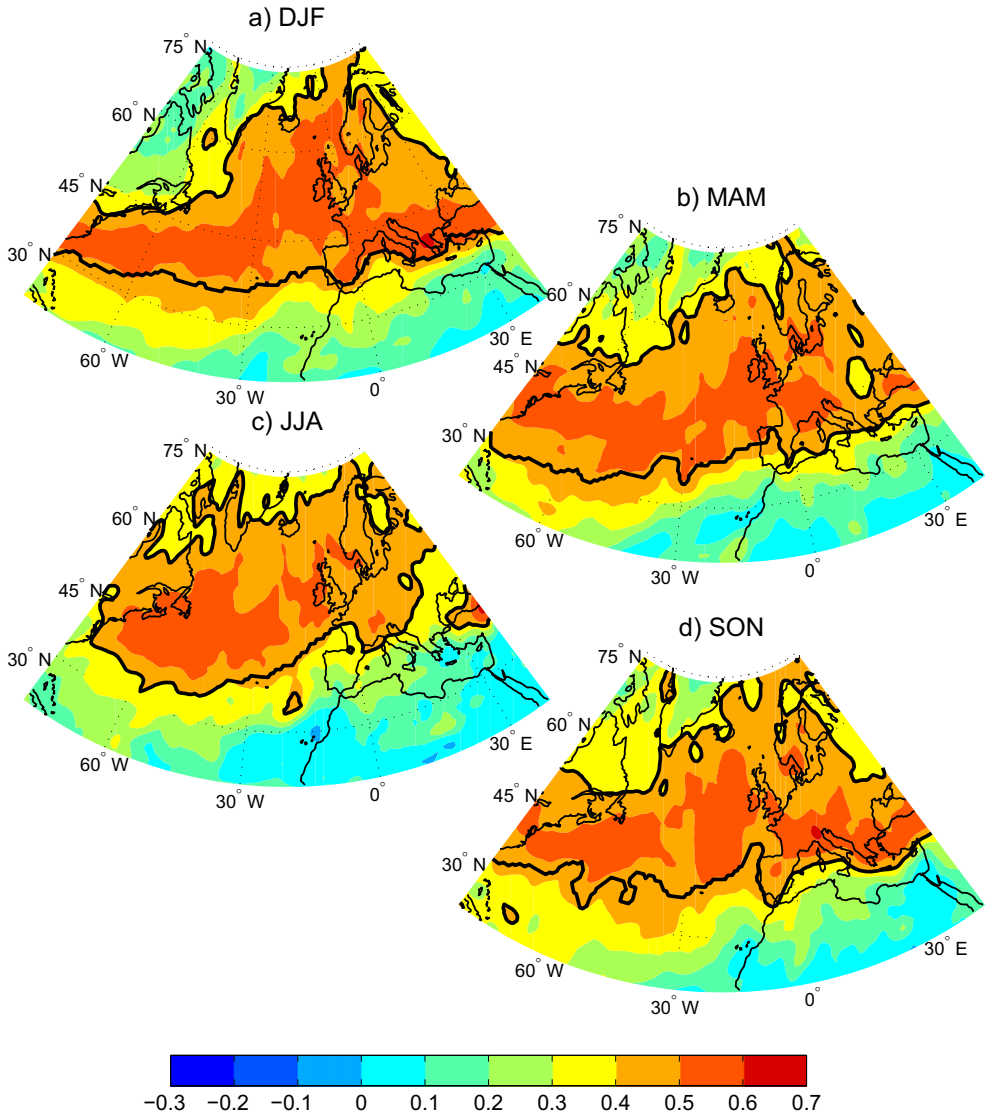

Fig. 12. Correlation (Pearson) between VRS instability (at 00, 06, 12 and 18 UTC) and total accumulated precipitation over the following 3h using all data from 1979 to 2010; a) DJF, b) MAM, c) JJA and d) SON. The thick black contour encloses regions where both the correlation > 0.4 and where the correlation with precipitation is stronger for VRS instability than it is for SCAPE.

paper to understand and quantify the relationship between metrics for the release of CSI and precipitation in a climatological context.

Typical features of SCAPE distributions in mature extratropical cyclones were synthesised from case studies: cold fronts are typically collocated with regions where CSI release is expected (inferred from large values of SCAPE, but small values of CAPE), whereas CSI release is not diagnosed as occurring in warm fronts and cold sectors (although SCAPE in these regions may have been underestimated by the SCAPE diagnostic used). Seasonal climatologies of SCAPE and CAPE demonstrated that the Gulf Stream region is a "hot-spot" for CSI with mean SCAPE values more than triple mean CAPE values in winter. This finding is consistent with Czaja and Blunt (2011) who, by comparing the moist entropy of the sea surface with that of the dynamical tropopause, concluded that CSI release is an important mechanism for modulating the tropospheric stratification from the sea surface temperature over the Gulf Stream.

The relative climatological distributions motivated the calculation of further instability and precipitation correlation statistics across the whole of the North Atlantic (using ERA-Interim data for both instability and precipitation). The correlation of SCAPE with precipitation was found to exceed that of CAPE with precipitation in the vicinity of the Gulf stream across most of the North Atlantic suggesting that SCAPE is capturing an additional aspect of the processes that modulate precipitation compared to CAPE. This hypothesis was supported by the correlations calculated between precipitation and regions where CSI was likely to actually be released as measured by the VRS instability (rather than just where CSI existed as measured by SCAPE). Regions where CSI is likely to be released are fairly common, occurring around 20% of the time over depths of around 1 km over the Gulf Stream region. Potential implications of poorly resolved CSI regions were discussed in the context of seasonal and decadal prediction and regional climate downscaling.

Acknowledgments

This paper is based on the PhD thesis of the first author which was funded by the Natural Environment Research Council (NE/H524865/1). Thanks are due to Bob Plant for the discussions and advice received during monitoring committee meetings and thesis revision period.

The ERA-I dataset used is available from http://www.ecmwf.int/en/research/climate-reanalysis/era-interim and the HadUKP dataset is available from http://www.metoffice.gov.uk/hadobs/hadukp/.

References

Alexander, L.V., Jones, P.D., 2001. Updated precipitation series for the UK and discussion of recent extremes. Atmos. Sci. Lett. 1, 142–150.

Bader, J.M., Forbes, G.S., Grant, J.R., Lilley, R.B.E., Waters, A.J., 1995. Images in Weather Forecasting. Cambridge University Press.

Balasubramanian, G., Yau, M.K., 1994. Baroclinic instability in a two-layer model with parameterized slantwise convection. J. Atmos. Sci. 51, 971–990.

Bennetts, D.A., Hoskins, B.J., 1979. Conditional symmetric instability - a possible explanation for frontal rainbands. Q. J. R. Meteorol. Soc. 105, 945–962.

Bennetts, D.A., Sharp, J.C., 1982. The relevance of conditional symmetric instability to the prediction of mesoscale frontal rainbands. Q. J. R. Meteorol. Soc. 108, 595–602.

Berrisford, P., Dee, D., Fielding, K., Fuentes, M., Kallberg, P., Kobayashi, S., Uppala, S., 2009. The ERA interim archive. ERA report series 1. . Technical ReportEuropean Centre for Medium-Range Weather Forecasts: Reading, UK.

Browning, K.A., 2004. The sting at the end of the tail: damaging winds associated with extratropical cyclones. Q. J. R. Meteorol. Soc. 130, 375–399.

Browning, K.A., Chapman, D., Dixon, R.S., 2001. Stacked slantwise convective circulations. Q. J. R. Meteorol. Soc. 127, 2513–2536.

Czaja, A., Blunt, N., 2011. A new mechanism for ocean-atmosphere coupling in midlatitudes. Q. J. R. Meteorol. Soc. 136, 2764–2785.

de Leeuw, J., Methven, J., Blackburn, M., 2014. Evaluation of ERA-interim reanalysis precipitation products using England and Wales observations. Q. J. R. Meteorol. Soc. 128, 839–859.

Dee, D.P., Uppala, S.M., Simmons, A.J., Berrisford, P., Poli, P., Kobayashi, S., Andrae, U., Balmaseda, M.A., Balsamo, G., Bauer, P., Bechtold, P., Beljaars, A.C.M., L., van de Berg, Bidlot, J., Bormann, N., Delsol, C., Dragani, R., Fuentes, M., Geer, A.J., Haimberger, L., Healy, S.B., Hersbach, H., Holm, E.V., Isaksen, L., Kallberg, P., Koehler, M., Matricardi, M., McNally, A.P., Monge-Sanz, B.M., Morcrette, J.J., Park, B.K., Peubey, C., de Rosnay, P., Tavolato, C., Thepaut, J.N., Vitart, F., 2011. The ERA-interim reanalysis: configuration and performance of the data assimilation system. Q. J. R. Meteorol. Soc. 137, 553–597.

Dixon, R.S., Browning, K.A., Shutts, G.J., 2002. The relation of moist symmetric instability and upper-level potential-vorticity anomalies to the observed evolution of cloud heads. Q. J. R. Meteorol. Soc. 128, 839–859.

Emanuel, K.A., 1983. On assessing local conditional symmetric instability from atmospheric soundings. Mon. Wea. Rev. 111, 2016–2033.

Emanuel, K.A., 1994. Atmospheric Convection. Oxford University Press.

Glinton, M.R., 2013. The Role of Conditional Symmetric Instability in Numerical Weather Prediction. Department of Meteorology - University of Reading. (Ph.D. thesis) available from http://www.met.reading.ac.uk/Library/phdsearch.html.

Gray, S.L., Martínez-Alvarado, O., Baker, L.H., Clark, P.A., 2011. Conditional symmetric instability in sting-jet storms. Q. J. R. Meteorol. Soc. 137, 1482–1500.

Gray, S.L., Thorpe, A.J., 2001. Parcel theory in three dimensions and the calculation of SCAPE. Mon. Wea. Rev. 129, 1656–1672.

Hobbs, P.V., 1978. Organization and structure of clouds and precipitation on the mesoscale and microscale in cyclonic storms. Rev. Geophys. 16 (4), 741–755.

Holley, D.M., Dorling, S.R., Steele, C.J., Earl, N., 2014. A climatology of convective available potential energy in Great Britain. Int. J. Climatol. 34 (14), 3811–3824.

Kendon, E.J., Roberts, N.M., Senior, C.A., Roberts, M.J., 2012. Realism of rainfall in a very high-resolution regional climate model. J. Clim. 25, 57915806.

Korty, R.L., Schneider, T., 2007. A climatology of the tropospheric thermal stratification using saturation potential vorticity. J. of Clim. 20, 5977–5991.

Lean, H.W., Clark, P.A., 2003. The effects of changing resolution on mesocale modelling of line convection and slantwise circulations in FASTEX IOP16. Q. J. R. Meteorol. Soc. 129, 2255–2278.

Lindstrom, S.S., Nordeng, T.E., 1992. Parameterized slantwise convection in a numerical model. Mon. Wea. Rev. 120, 742–756.

MacLachlan, C., Arribas, A., Peterson, K.A., Maidens, A., Fereday, D., Scaife, A.A., Gordon, M., Vellinga, M., Williams, A., Comer, R.E., Camp, J., Xavier, P., Madec, G., 2015. Global seasonal forecast system version 5 (GloSea5): a high-resolution seasonal forecast system. Q. J. R. Meteorol. Soc. 141, 1072–1084.

Meukaleuni, C., Lenouo, A., Monkam, D., 2016. Climatology of convective available potential energy (CAPE) in ERA-Interim reanalysis over West Africa. Atmos. Sci. Lett. 17, 65–70.

Monkam, D., 2002. Convective available potential energy in Northern Africa and tropical atlantic and study of its connection with rainfall in Central and West Africa during summer 1985. Atmos. Res. 62, 125–147.

Morcrette, C.J., 2004. Radar and Modelling Studies of Upright and Slantwise Convection. University of Reading, (Ph.D. thesis) available from http://www.met.reading.ac.uk/Library/phdsearch.html.

Novak, D.R., Colle, B.A., Aiyyer, A.R., 2010. Evolution of mesoscale precipitation band environments within the comma head of northeast U.S. cyclones. Mon. Wea. Rev. 138, 2354–2374.

Ooyama, K., 1966. On the stability of the baroclinic circular vortex: a sufficient criterion for instability. J. Atmos. Sci. 23, 43–53.

Persson, P.O.G., Warner, T.T., 1991. Model generation of spurious gravity waves due to inconsistency of the vertical and horizontal resolution. Mon. Wea. Rev. 121, 1821–1833.

Riemann-Campe, K., Fraedrich, K., Lunkeit, F., 2009. Global climatology of convective available potential energy (CAPE) and convective inhibition (CIN) in ERA-40 reanalysis. Atmos. Res. 93 (1), 534–545.

Romero, R., Gayà, M., Doswell, C.A., 2007. European climatology of severe convective storm environmental parameters: a test for significant tornado events. Atmos. Res. 83 (2), 389–404.

Schultz, D.M., Schumacher, P.N., 1999. The use and misuse of conditional symmetric instability. Mon. Wea. Rev. 127 (12), 2709–2732.

Sheldon, L., 2015. The role of deep moist convective processes in western boundary currents - troposphere coupling. Department of Physics - Imperial Collage, London. (Ph.D. thesis)

Shutts, G.J., 1990a. Dynamical aspects of the October storm, 1987: a study of a successful fine-mesh simulation. Q. J. R. Meteorol. Soc. 116 (496), 1315–1347.

Shutts, G.J., 1990b. SCAPE charts from numerical weather prediction model fields. Mon. Wea. Rev. 118 (12), 2745–2751.

Smith, R.N.B., 1990. A scheme for prediction layer cloud and their water content in a general circulation model. Q. J. R. Meteorol. Soc. 116, 435–460.

Stone, P.H., 1966. On non-geostrophic baroclinic stability. J. Atmos. Sci. 23, 390–400.

Subrahmanyam, K.V., Kumar, K.K., Babu, A.N., 2015. Phase relation between CAPE and precipitation at diurnal scales over the Indian summer monsoon region. Atmos. Sci. Lett. 16, 346–354.

Thorpe, A.J., Emanuel, K.A., 1985. Frontogenesis in the presence of small stability to slantwise convection. J. Atmos. Sci. 42 (17), 1809–1824.

Wigley, T.M.L., Lough, J.M., Jones, P.D., 1984. Spatial patterns of precipitation in England and Wales and a reviesed homogeneous England and Wales precipitation series. Int. J. Climatol. 4, 1–25.

Xu, Q., Clark, J.H.E., 1985. The nature of symmetric instability and its similarity to convective and inertial instability. J. Atmos. Sci. 42, 2880–2883.

Zawadzi, I., Torlaschi, E., Sauvageau, R., 1981. The relationship between mesoscale thermodynamic variables and convective precipitation. J. Atmos. Sci. 38, 1535–1540.